NASA Technical Paper 1111

Effects of Entrained Water and Strong Turbulence on Afterburning Within Solid Rocket Motor Plumes

Richard I. Gomberg and Richard G. Wilmoth

JANUARY 1978

NASA

NASA Technical Paper 1111

Effects of Entrained Water and Strong Turbulence on Afterburning Within Solid Rocket Motor Plumes

Richard I. Gomberg and Richard G. Wilmoth
Langley Research Center
Hampton, Virginia

National Aeronautics
and Space Administration

**Scientific and Technical
Information Office**

1978

SUMMARY

During the first few seconds of the space shuttle trajectory, the solid rocket boosters will be in the proximity of the launch pad. Because of the launch pad structures and the surface of the Earth, the turbulent mixing experienced by the exhaust gases will be greatly increased over that for the free-flight situation. In addition, a system will be present, designed to protect the lifting vehicle from launch structure vibrations, which will inject large quantities of liquid water into the hot plume. This report studies the effects of these two phenomena on the temperatures, chemical composition, and flow field present in the afterburning solid rocket motor exhaust plumes of the space shuttle. The study includes results from both a computational model of the afterburning and supporting measurements from Titan III exhaust plumes taken at Kennedy Space Center with infrared scanning radiometers.

INTRODUCTION

As part of a continuing assessment of the environmental effects of space shuttle operations, the National Aeronautics and Space Administration has been studying the formation and behavior of rocket exhaust clouds from solid propellant rocket motors. Although information is readily available as to the composition of the rocket exhaust as it leaves the motor's nozzle exit plane (see, for example, ref. 1), significant changes occur in the composition of the plume as these hot exhaust products afterburn in the atmosphere. An understanding of these afterburning processes is necessary so that a reliable source term can be formed which will serve as input to diffusion models and form a basis for determining which products are of ecological significance. The purpose of this study is to predict a source term for those exhaust products which are released in the proximity of the launch pad.

From free-flight calculations it is known that the solid propellant motors of the shuttle will release substantial quantities of such gases as HCl and NO into the troposphere and that material released below the local inversion layer will rise to form a stabilized exhaust cloud. Approximately two-thirds of this material is released in plumes whose afterburning properties can be said to occur under free-flight conditions. The remaining material is released close enough to the ground and launch pad structures to necessitate a separate consideration of afterburning with boundary conditions distinct from those of free flight.

Studies of the afterburning processes occurring within the plumes of the Titan III and shuttle solid rocket motors in free flight were reported in references 2 and 3. These studies included temperature and velocity distributions within the plume as well as an analysis of the major chemical constituents. The altitude range considered in these studies was from 0.7 to 15 km. Below an altitude of roughly 0.5 km, free-flight turbulent mixing rates and ordinary atmospheric boundary conditions can no longer be considered valid. The

interaction of the exhaust plume with the launch pad structures, the flame trench and associated "deluge" water, and the Earth's surface may all have major effects on afterburning.

The differences between afterburning near the launch pad and in free flight that are considered in this study can be classified into two main categories. The first is that the rate of turbulent mixing of air into the plume is significantly increased as a result of the gases which flow out of the nozzle and hit the pad deflectors and structures. The other significant occurrence which affects only early launch afterburning of the space shuttle is the initiation at a few seconds before lift-off of the so-called "acoustic water suppression system." This acoustic water system is described in figure 1. The basic purpose of the system is to protect the vehicle from vibrations in the launch pad structures caused by strong vibrations set up by the motors of the shuttle boosters. These vibrations are to be suppressed by injecting large quantities of water into the gas flow from the motor. This injection will occur near the firing pad and in the flame trench. The flame trench is a large open pit reinforced by concrete which runs under the firing pad and which channels the afterburning gases away from the launch area. For the space shuttle, the solid rocket motor gases will travel a path through the trench which is about 80 m in length.

Present plans are that at 4 seconds before launch water will be injected under the firing pad and into the flame trench at a rate of 16 000 ℓ/sec on the solid motor side (fig. 1) until at least 8 seconds after lift-off. This rate represents a mass flow rate of about 16 000 kg/sec from lift-off through this period; and a large percentage of this flow will be entrained into the plume. The mass flow rate of the plume is somewhat less than this rate, being roughly 10 000 kg/sec.

Although the effect of water injection on afterburning occurs primarily through temperature quenching, the effect is also closely coupled to the turbulent mixing processes. Since modifications to the basic physical model are required to account for this two-phase flow, the water injection problem was studied first. The following sections describe the basic numerical plume model and the development of a simple kinetic rate model for water injection. Results showing the effects of entrained water on afterburning are presented along with an assessment of the accuracy of the water injection model. Correlations are then made with scanning infrared radiometer photographs of actual Titan III plumes to determine the magnitude and effects of the enhanced turbulent mixing based on a simple mixing length model.

SYMBOLS

A	area of plume
a	speed of sound
C	rate of radius of droplet reduction
D	diffusion coefficient of water in air near droplet

$f(\ )$	function
K	thermal conductivity
k_f	forward reaction rate
L	heat of vaporization of water
M	arbitrary third body in a three body reduction, also Mach number
m	mass
N_A	Avogadro's number
p_r	pressure at droplet surface
p_∞	pressure far from droplet surface
R	radius of nozzle
R_g	universal gas constant
r	radius of water droplet
r_f	radius of droplet at final time t_f
r_o	radius of droplet at time $t = 0$
T	temperature
t	time
t_f	final time
U,u	velocity of plume gases
W_{mix}	molecular weight of mixture of exhaust gases and air
X	mole fraction; subscript denotes compound
y	distance measured radially
α	scaling factor for viscosity
μ	cofficient of viscosity
ρ_{mix}	density of mixture of exhaust gases and air
ρ_r	density of water at droplet surface
ρ_∞	density of water far from droplet surface

Subscripts:

c	inner core
dv	developed region of mixing
r	at radius of droplet
∞	far beyond radius of droplet

MODEL DEVELOPMENT

Basic Numerical Model

The basic numerical model used to simulate the afterburning processes is the low-altitude plume program (LAPP) code. (See ref. 4.) This is a steady-state axisymmetric code which couples the effect of kinetic rate chemistry to turbulently mixing fluid flows. The code uses an explicit-implicit finite-differencing scheme to "march" downstream of the nozzle exit plane.

As inputs to the code, it is necessary to specify the conditions at the nozzle exit plane as well as the conditions of the unperturbed atmosphere into which the nozzle gases are flowing. The number of species in the plume, the chemical reactions which they undergo, and the reaction rate coefficients must be included. It is also necessary to specify the rate of turbulent mixing.

The LAPP code contains several options for turbulent mixing models. The model used in this study is the Donaldson-Gray model (ref. 5) which was chosen because of its successful use in prior studies (ref. 6). The Donaldson-Gray model contains an undetermined mixing coefficient which is usually set equal to unity under tropospheric free-flight conditions. This parameter is referred to as α. Later in this study, a reasonable value for this coefficient in the highly turbulent flow near the launch pad was determined.

As discussed in the "Introduction," water is injected into structures beneath the pad at a rate of 16 000 kg/sec starting at 4 seconds prior to launch. When the actual firing of the solid motors occurs, these gases will essentially be flowing into a "lake" of water. Much of the water will be entrained into the plume which, in turn, will vaporize the water into steam. This highly endothermic vaporization reaction (2261 J/g) will tend to quench some of the high temperature afterburning.

In figure 2 the importance of the phase change is shown for the preliminary case of a plume whose exit plane constituents are precisely those of a shuttle SRM, but where no chemical reactions are allowed to take place. In this inert plume, all cooling takes place by the mixing of a cool substance with a warm substance and only nonchemical heat transfer takes place. In the calculations leading up to this figure, the phase change was included by using an early thermodynamic equilibrium model. In this figure is plotted the temperature along the plume center line as a function of distance downstream of

the nozzle exit plane. As can be seen, where the phase change was present (with liquid water in the atmosphere), the cooling took place significantly faster than with air only or air plus water vapor. It was thus considered important to treat the phase change in any set of detailed calculations.

The LAPP code makes the assumption that all substances in the plume are ideal gases. Clearly, for the study under consideration where liquid water is vaporized, such a single phase model is inadequate. After investigating several alternate approaches, it was decided to include the effects of the acoustic suppression water by having a mixture of air and liquid water entrained into the plume in the first 80 m (the path length of the flow field from the nozzle at the pad through the flame trench) and entraining pure air from 80 m until the problem terminates about 1 km downstream of the exit plane.

To account for the phase change during evaporation, liquid water is considered a new chemical species which obeys the equation of state of a perfect gas as required by the code, but with thermodynamic properties (heat capacity, specific enthalpy, etc.) appropriate to liquid water below 373 K and appropriate to water vapor above 373 K. The heat of vaporization is included by means of an imaginary chemical reaction:

$$\text{Liquid water} + M \xrightarrow[\text{irreversibly}]{} H_2O + M \qquad (1a)$$

This reaction is endothermic, 40.70 kJ/mole, which is the heat of vaporization of a mole of liquid water. M is an arbitrary third body.

It was found during the course of the investigation that because of the preponderance and stability of the N_2 molecule,

$$\text{Liquid water} + N_2 \xrightarrow[\text{irreversibly}]{} H_2O + N_2 \qquad (1b)$$

could be used with negligible differences in the results.

Rate Coefficient Calculation

In addition to specifying the constituents of a reaction, it is also necessary to denote the value of the reaction rate coefficient appropriate to the reaction. The reaction rate coefficient appropriate to equation (1b) is calculated as follows:

Let $X_{\text{liquid water}}$ equal the mole fraction of liquid water and X_{N_2} equal the mole fraction of N_2. From the formulation of the chemistry in the LAPP code (ref. 4), it can be deduced that

$$X_{\text{liquid water}}(t) = X_{\text{liquid water}}(T = 0) \exp\left[-N_A k_f(T) \frac{\rho_{mix}}{W_{mix}} X_{N_2} t\right]$$

where N_A is Avogadro's number, $k_f(T)$ is the unknown forward reaction rate coefficient dependent upon temperature T, t is time, ρ_{mix} is the density of the mixture, and W_{mix} is the molecular weight of the mixture of plume gases, air, and water.

Throughout the wide range of physical and thermodynamic conditions encountered in this study, it was invariably found that the overwhelming preponderence of liquid to vapor transition occurred in the stream tube most distant from the center line with a temperature above 373 K. It was further observed that many quantities in the stream tube were relatively constant. For example, W_{mix} stays within 10 percent of 27 g/mole, ρ_{mix} stays within 10 percent of 1 mg/cm^3, and X_{N_2} stays within 20 percent of 0.8. These results hold for all values of downstream distance. Using these values simplifies the rate expression to

$$X_{\text{liquid water}}(t) \stackrel{o}{=} X_{\text{liquid water}}(T = 0) \exp\{-k_f(T)\ 1.8 \times 10^{19}\ t\}$$

Since more than 98 percent of all vaporization takes place in the outermost stream tube at a temperature of approximately 373 K, it is not surprising that once the value of k_f is fixed in this stream tube, the behavior of the plume is relatively insensitive to the temperature dependence of k_f in the higher temperature stream tubes. Several different forms of $k_f(T)$ were tried and included:

$$k_f(T) = k_f(373\ K)\sqrt{T} \tag{2}$$

$$k_f(T) = k_f(373\ K)T \tag{3}$$

$$k_f(T) = k_f(373\ K)T^2 \tag{4}$$

Using equations (3) and (4) was found to be somewhat more expensive computationally than using equation (2) and did not affect plume behavior significantly. Hence, $k_f(T) = k_f(373\ K)\sqrt{T}$ (eq. (2)) was used throughout the study.

By using the form of the rate coefficient described and assuming a value for $k_f(373\ K)$, the model predicts a specific "e-folding" time (or time to reach 1/e times its original value) for water evaporation at every point in the flow field. Examples of these times are given in table I. To determine the proper value of $k_f(373\ K)$, it is necessary to have some idea of what the true e-folding time is for water droplets evaporating in this situation. This question is treated in the next section.

Heat and Mass Transfer in Water Droplets

In this section an attempt is made to predict the rate of evaporation of water droplets. This study follows closely the techniques developed in reference 7. The basic assumptions in this calculation are that (1) the heat flowing into the droplet from the carrier gas is equal to the heat lost by the

droplet through evaporation, and (2) the mass flow from the droplet can be viewed as a diffusion process.

The heat transferred into a droplet of radius r with thermal conductivity K, and a surface temperature T_r from a carrier gas with temperature T_∞ will be given by $4\pi Kr(T_\infty - T_r)$. Equating this relation to the heat lost by the droplet through evaporation

$$-L \frac{dm}{dt} = 4\pi Kr(T_\infty - T_r) \tag{6}$$

where L is the heat of vaporization of the water.

If water molecules are thought of as leaving the surface as a result of a diffusion process, then

$$- \frac{dm}{dt} = 4\pi rD(\rho_r - \rho_\infty) \tag{7}$$

where D is the diffusion coefficient of water in air near the droplet, ρ_r is the density of water at the surface of the droplet, and ρ_∞ is the density of water at a distance large compared with r.

This model neglects the phenomenon of surface tension and possible spallation of the droplet. Since the LAPP code assumes all particles and gases flow at the same speed in each stream tube, conduction effects are also neglected. The technique just described is most appropriate for a quiescent moderate temperature medium rather than the hot turbulent edge of a rocket plume. Nevertheless, since diffusion and heat transfer within the droplet are dominant processes, the resultant e-folding time should be reasonable.

Equating dm/dt in equations (6) and (7) and using the ideal gas equation to define ρ_r and ρ_∞ results in the following equation:

$$\frac{K(T_\infty - T_r)}{L} = D(\rho_r - \rho_\infty) = \frac{D}{R_g}\left(\frac{p_r}{T_r} - \frac{p_\infty}{T_\infty}\right) \tag{8}$$

where

$K = 2.6 \times 10^{-4}$ J/cm-K-sec

R_g = Gas constant

$$L = 2.26 \times 10^3 \text{ J/g}$$

$$D = 0.219 \text{ cm}^2/\text{sec}$$

The quantity p_∞/T_∞ is assumed small compared with P_r/T_r and the term is dropped.

The undetermined quantity is T_r or more appropriately $T_r - T_\infty$, the driving force behind the heat transfer.

By assuming that p_r is the saturation vapor pressure of water at the droplet temperature T_r, and by consulting appropriate vapor pressure tables, $T_r - T_\infty$ is found to be about 85 K.

By assuming a particle density of 1 g/cm^3 for water, equation (6) becomes

$$-Lr \frac{dr}{dt} = k(T_\infty - T_r) \tag{9}$$

Under the assumptions that L, K, and $T_\infty - T_r$ are constant with respect to time, integration of equation (9) implies that

$$r^2 = r_o^2 - Ct \tag{10}$$

where

$$C = \frac{2k(T_\infty - T_r)}{L} \tag{11}$$

In this case

$$C = 1956 \ (\mu m)^2/\text{sec}$$

As a working definition of evaporation, a droplet will be said to have evaporated when its volume has reached approximately 1 percent of its original volume. Since $e^{-4} = 0.01$, this condition corresponds to 4 e-folding times. In terms of radii

$$r_o = \sqrt[3]{100}\, r_f = 4.65 r_f \tag{12}$$

Equations (10) to (12) lead to the conclusion that the rate of evaporation depends on the initial size of the droplet. In table II is presented the evaporation time as calculated from these equations as a function of initial particle radius.

Water droplets from spray nozzles such as the ones used in the acoustic suppression system generally range anywhere from 10 μm to 0.5 cm. As shown in table II, this value corresponds to evaporation times from 50 msec to extremely long times. In the system at Kennedy Space Center the large end of the droplet size spectrum will probably be dominant. By comparing the e-folding times in table I with the values in table II, the appropriate rate coefficients are deduced as $10^{-18}\sqrt{T}$ or lower.

These results must be used with a great deal of caution. For particles larger than a few hundred micrometers, the moving of mass away from the water droplet by diffusion is a severe limitation. The medium in which the particles move is in turbulent motion, large thermal gradients exist in the regions under consideration - far larger than the difference between droplet temperatures and 373 K - and collisions occur. All these effects are neglected in the heat flow and diffusion calculation made.

For this reason, error bands of a factor of 10^3 are put on the value of k_f, and the water entrainment effects were studied with $k_f(373\ K)$ as high as 10^{-14} and as low as 10^{-20}. Most attempts to run the calculation with $k_f(373\ K)$ higher than 10^{-14} were frustrated by the prohibitive amount of computer time necessary to run these faster cases. Since large droplet sizes are anticipated, the lower rate coefficients will apply to most droplets.

MODELING RESULTS

Water Entrainment Calculation

Four cases of acoustic water injection were studied. The first was an excess water flow condition which is appropriate for the initial firing where there is a large excess of water in the flame trench. Here a mass flow of water equal to twice the mass flow of the exhaust gases is entrained into the plume in the first 20 m. Another case studied was the matched flow condition where the amount of water entrained was equal in mass flow to the exhaust gas flow. This is roughly appropriate for a few seconds after lift-off. Cases for one-half and one-quarter of the mass flow of the gas were also studied. In every case an additional one-third of the value of mass flow is entrained from 20 to 80 m because of additional water injection.

Among the primary effects of the suppression of afterburning as a result of the quenching water is that increased amounts of carbon monoxide survive the afterburning process over the free-flight case. To obtain an estimate of this increase that would tend to be conservative from an environmental or safety standpoint, the high value of $k_f(373\ K) = 10^{-16}$ was used in a detailed set of calculations. The chemical reaction scheme besides that of the water evaporation reaction consists of 22 reactions involving 18 chemical species. These reactions and their rate coefficients are presented in table III.

The nozzle exit plane conditions used in this study are given in table IV. An entrainment coefficient of $\alpha = 1$ was used in this study which, as will be seen, slightly underestimates the rate of entrainment of water, but does not

cause great errors in the final results. The results are shown in two forms. The form of major importance introduces the concept of number of grams of species per downstream meter of plume. As the gases flow downstream of the exit plane, they entrain cool air and water and they react chemically. As the entrainment process proceeds downstream, the gases rapidly cool to the ambient temperature and slow to the speed of the air (in the frame of reference of the motor). As the gases cool, the kinetic reactions slow considerably so that several hundred meters downstream of the exit plane, the chemical reactions are proceeding at a rate that is negligible in comparison with the rate at the exit plane. If one were to take a cross-sectional slab of the plume in the radial direction with a thickness of 1 m in the downstream direction at some distance downstream, such a volume would contain so many grams of HCl, so many grams of CO_2, etc. The number of grams of such a species per downstream meter of plume gives one an estimate of the quantity of species being deposited in the cool, slowly reacting region of the rocket plume.

Table V is such a list of species for a distance of 1 km downstream of the exit plane for the cases delineated. There are several things to notice in this table. The amount of carbon monoxide in the plume that does survive afterburning gets larger as the amount of entrained water increases. However, for the mass flows of water considered, at no time are there particularly large quantities of carbon monoxide, at least when using $k_f(373\ K) = 10^{-16}$. Another point to recognize from this table is that the amount of Al_2O_3 fluctuates slightly. In the model of afterburning being considered here, Al_2O_3 is an inert quantity. Hence, the quantity

$$(\rho UA)_{Al_2O_3} = \text{Constant}$$

That is, its mass flow must remain constant. If, as one would expect, at 1 km from the exit plane, the speed of the aluminum oxide particles is roughly the same for all cases of water entrainment, then the amount of Al_2O_3 in g/m must also be approximately the same. The table bears this conjecture out, the small relative variations in Al_2O_3 being due more to "noise" in the numerical scheme than true speed variations. (See ref. 3.) The small percentage variations in the quantity of CO_2 may also be considered numerical "noise" variations except for that effect of the nonconversion of CO to CO_2 during suppressed afterburning.

On the other hand, the large relative drop in the production of nitric oxide with increasing amounts of deluge water is due to the quenching of afterburning. Similarly, the production of Cl_2 from HCl falls off for the same reason. The success of these large amounts of water in suppressing the high temperature region is shown in figure 3. This figure shows center-line temperature as a function of downstream distance for the various cases. The temperature never exceeds that of the nozzle exit plane for the excess flow case; whereas with unquenched afterburning, temperatures rise several hundred degrees above that of the exit plane.

In figure 4 is shown the chlorine partitioning of the plume among the various possible species present along the center line of the plume. The decrease of all concentrations of chlorine-containing species at large distances downstream of the exit plane is due to dilution rather than to afterburning.

In figure 5 a similar plot is made for combustion species. Here are plotted the mole fractions of H_2, CO, H_2O, liquid water, CO_2, and OH in the plume as a function of the distance downstream from the nozzle exit plane. As can be seen, as afterburning proceeds, the initially dominant concentration of CO drops as its molecules move downstream and are oxidized to become CO_2. The small quantities of CO which appear at large distances are entrained from those regions of the plume in which CO is not completely burned. As can be seen from this figure, the concentrations of H and OH drop off rapidly as they combine to form water vapor. In figures 6 and 7 the same chemical species are shown in g/m. (Liquid water is not shown in this graph because its value quickly becomes too large.) The asymptotic values of these curves represent the quantities of species deposited in the low temperature regions of the plume.

It should be noted also that in the various cases considered, larger and larger amounts of liquid water are vaporized. Consequently, more and more of the energy of the plume is used to vaporize the water; as a result, the amount of energy available for cloud buoyancy is reduced.

Sensitivity to Water Evaporation Rate Coefficient

In addition to the results obtained, a parametric study was undertaken to determine the sensitivity of these results to uncertainties in the evaporation reaction rate coefficient. The excess water flow situation was used as a test case. In this study the chemical scheme used was identical with that of table III except that the reaction rate coefficient of reaction (20) was varied as shown in table VI. The results of this study are also presented in this table. Again, as can be seen in the variation of Al_2O_3, variations of 3 percent or less must be considered physically meaningless. However, several overall trends can be ascertained from the results. As the rate coefficient for evaporation of water becomes larger, the amount of HCl increases at the expense of Cl_2; the amount of carbon monoxide that survives afterburning increases significantly; and the production of nitric oxide drops rapidly.

The temperature quenching resulting from the various water evaporation rate coefficients is illustrated in figure 8 by the center-line temperature variation along the plume. As can be seen, the larger rate coefficient reactions suppress afterburning strongly.

In figure 9 the quantity of chlorine-containing species (HCl and Cl_2) is plotted as a function of downstream distance for several water evaporation coefficients. As can be seen, the quantity of Cl_2 drops dramatically as the rate coefficient increases whereas HCl quantities remain essentially unchanged. In figure 10 the quantity of NO produced is seen to drop rapidly with increasing rate coefficient whereas CO production rises (fig. 11).

FIELD MEASUREMENTS OF PLUME TURBULENCE NEAR THE LAUNCH PAD

Another effect which the launch pad structures will have on low-altitude afterburning is to greatly increase the turbulent mixing occurring in the flow field over the free-flight mixing. Since this increase in turbulence will have

directly measurable effects on plume shape and temperatures, measurements of these parameters have been made with infrared scanners to determine the amount of mixing.

Infrared scanning radiometry of rocket exhaust clouds has become a standard part of the NASA launch vehicle effluents measurement techniques. Several commercially available radiometers sensitive to infrared radiation from 3 to 5.6 μm have been used to study the formation and diffusion of rocket exhaust clouds. The details of this measurement technique can be found in reference 8.

Much like a camera sensitive to visible radiation is able to form a television picture of moving objects at various radiant intensities, so can the output of a camera sensitive to infrared (heat) radiation be converted to images on a cathode ray tube (CRT). By studying the thermal heat patterns of the plume of a lifting rocket vehicle, it is possible to directly infer both mass and temperature distributions in the plume.

The heat pattern of a solid rocket motor plume which is in free flight is shown in figure 12. This infrared scan was taken of a Titan vehicle on March 14, 1976. The altitude of the vehicle is roughly 3 km. The horizontal white line in the picture is a marker which can measure intensities. The isotherm shown in the picture (the white vertical line in the center) is roughly an indication of 15 K above ambient or higher. By measuring the intensities along this plume, the isotherm indicating 100 K above ambient is present in the thick part at the top of the picture and is well within the thin vertical plume shown in the picture terminating about 1 km behind the nozzle exit plane.

In contrast to this free-flight behavior of a constantly narrowing 100 K above ambient isotherm, figure 13 was taken of a lifting Titan vehicle on May 20, 1975. The altitude of the vehicle is about 1.1 km. The plume shown is entirely the 100 K above ambient or higher isotherm. As can be seen, although the part of the plume from 1.1 km to near the pad is constant in width or even decreasing, once the plume hits the ground a noticeable spreading of this high temperature region occurs with a fairly abrupt termination not too far downstream of the area where the spreading first occurs.

This is shown in figure 14 in normal and downstream coordinates. Such behavior can be simulated on the computer by assuming more rapid turbulent mixing.

With the after-deflection flow field data such as those in figures 13 and 14 as guides, an analytical study of increased turbulence at the pad was undertaken. No attempt was made to develop a new theory of turbulent flow in this kind of situation. Several empirical models based on the concept of mixing length are available at the present time in LAPP. A reasonable formalism for the situation under study is given by Donaldson and Gray in reference 5. This model divides the flow field into an inner core flow and an outer developed flow. In the core region, the coefficient of viscosity

$$\mu = \alpha f_c(M,a,r,\rho,u)$$

where f_c is a function of local Mach number M, speed of sound a, radius of the region r, density ρ, and velocity u. In the developed region

$$\mu = \alpha f_{dv}(M,a,r,\rho,u)$$

where f_{dv} is a different function of the same variables. Thus α is a crucial parameter since it scales the mixing rate in both regions. The parameter α is set equal to unity in the free-flight case; for greater turbulence it attains higher values.

For the cases studied, the vehicle is on the launch pad and the nozzle exit plane is in the proximity of the flame trench. The turbulent mixing parameter α is assumed to be unity within the trench. From this point on until more than 1 km downstream of the exit plane, several different values of α were used in a parametric series of runs which included α = 1, 5, 10, 20, and 100. The values 20 and 100 are physically unrealistic in all but the most violent of mixing situations.

Consider now figure 15 in which is plotted the 400 K isotherm for the various cases of α used. Note that the use of $\alpha = 5$ from 80 m onward gives a fairly good representation of the measured isotherm (see figs. 13 and 14) in the downstream coordinate system. Based on this turbulence correlation with the infrared results for the full effects of the launch pad complex on afterburning, the most reliable results are obtained by using $\alpha = 5$.

The sensitivity of the center-line temperature to these turbulence variations is shown in figure 16. In this figure is plotted the center-line temperature of the plume as a function of distance downstream for several values of α. As can be seen, the more violent the turbulent mixing, the more quickly afterburning is terminated. The quenching for $\alpha = 5$ is seen to be much more rapid that for the free-flight case ($\alpha = 1$).

In table VII is shown the asymptotic values of the amount in g/m of various species produced. Again this condition represents the excess water case with $k_f(T) = 10^{-16}\sqrt{T}$. As α increases, CO and Cl_2 production increases and NO production seems to fall. All values have been normalized so that at a downstream distance of 1 km, the value of Al_2O_3 in g/m is the same in all cases.

In table VIII the combined effects of increased turbulence and excess water flow are contrasted with what would happen under the same nozzle exit plane conditions for the free-flight case.

CONCLUDING REMARKS

A computational model of the afterburning processes occurring in a space-shuttle-like solid rocket motor plume has been used to study the species composition and flow properties of the plume in the proximity of the launch pad. The model treats parallel turbulent mixing coupled with finite-rate chemistry between the plume and the ambient atmosphere. The principal perturbations considered are the temperature quenching due to injection of large quantities of water into the launch pad flame trench and the increased turbulence due to

both the injection of water and the proximity of the plume to the launch pad structures and the surface of the Earth.

The evaporation of the injected liquid water has been modeled as a kinetic rate process. A relation between the effective evaporation rate coefficient and the water droplet size has been estimated from heat and mass transport considerations. Afterburning calculations were then performed by using rate coefficients corresponding to droplet radii between 0.1 μm and slightly less than 100 μm for amounts of water entrained varying from 0.65 to 2.4 times the exit plume mass flow. Radii greater than these values are also considered. In all cases the predicted plume temperatures are significantly lower than those in the free-flight case due to the evaporation of water.

The increased turbulence near the launch pad has been modeled by varying the eddy viscosity coefficient in the turbulent mixing models. Correlations were then made between the predicted 100 K above ambient isotherm and that measured with a scanning infrared radiometer of a Titan III exhaust plume. These correlations show that increasing the eddy viscosity coefficient by a factor of 5 over that used in the free-flight case gives a reasonably good representation of the measured spreading rate for the 100 K above ambient isotherm.

The principal afterburning species affected by the water injection and increased turbulence were found to be Cl_2, CO, and NO. The combined effects of increased turbulence and injected water flow twice that of the mass flow through the nozzle exit plane are to suppress NO production almost completely, to lower the amount of Cl_2 produced in the plume over free-flight conditions, and correspondingly increase slightly the HCl production. In addition, these effects will produce larger amounts of CO than in the free-flight case, but the ratio of CO_2 to CO will still be on the order of a hundred to one.

Langley Research Center
National Aeronautics and Space Administration
Hampton, VA 23665
December 2, 1977

REFERENCES

1. Solid Propellant Engineering Staff: Nozzle Exit Exhaust Products From Space Shuttle Boost Vehicle (November 1973 Design). Tech. Memo. 33-712, Jet Propulsion Labs., California Inst. Technol., Feb. 1975. (Available as NASA CR-136747.)

2. Stewart, Roger B.; and Gomberg, Richard I.: The Production of Nitric Oxide in the Trosposphere as a Result of Solid-Rocket-Motor Afterburning. NASA TN D-8137, 1976.

3. Gomberg, Richard I.; and Stewart, Roger B.: A Computer Simulation of the Afterburning Processes Occurring Within Solid Rocket Motor Plumes in the Troposphere. NASA TN D-8303, 1976.

4. Mikatarian, R. R.; and Pergament, H. S.: Aerochem Axisymmetric Mixing With Nonequilibrium Chemistry Computer Program. TP-200 (Contract AF 04(611)-11541), AeroChem Res. Lab., Inc., June 1969. (Available from DDC as AD 856 017.)

5. Donaldson, Coleman duP.; and Gray, K. Evan: Theoretical and Experimental Investigation of the Compressible Free Mixing of Two Dissimilar Gases. AIAA J., vol. 4, no. 11, Nov. 1966, pp. 2017-2025.

6. Pergament, H. S.; and Mikatarian, R. R.: Prediction of Minuteman Exhaust Plume Electrical Properties. AFRPL-TR-72-129, U.S. Air Force, July 1973.

7. Myers, Richard Lee: Electrical Detection of Airborne Particulates Using Surface Ionization Techniques. Ph. D. Thesis, University of Pittsburgh, 1973. (Also available as SRCC Rep. No. 193, Univ. Pittsburgh, Aug. 1973.)

8. Gomberg, Richard I.; Kantsios, Andronicos G.; and Rosensteel Frederick J.: Some Physical and Thermodynamic Properties of Rocket Exhaust Clouds Measured With Infrared Scanners. NASA TP-1041, 1977.

TABLE I.- RESULTANT e-FOLDING DROPLETS DECAY TIMES AS A FUNCTION OF KINETIC RATE COEFFICIENT

[T is assumed to be 373 K]

Assumed k_f(373 K)	10^{-20}	10^{-17}	10^{-16}	10^{-15}	10^{-14}
Resultant e-folding time, sec	4×10^{-1}	4×10^{-4}	4×10^{-5}	4×10^{-6}	4×10^{-7}

TABLE II.- DROPLET EVAPORATION TIMES (4 e-FOLDING TIMES) AS PREDICTED BY THE DIFFUSION - HEAT FLUX MODEL

Initial droplet radius, μm	100	10	1	0.1
Evaporation times, sec	5	5×10^{-2}	5×10^{-4}	5×10^{-6}

TABLE III.- CHEMICAL SCHEME[a]

Reaction	Rate coefficient
(1) $H + Cl + M = HCl + M$	$3 \times 10^{-29}T^{-1}$
(2) $H + HCl = Cl + H_2$	$8.8 \times 10^{-11} \exp(-4\ 622/R_gT)$
(3) $HCl + OH = H_2O + Cl$	$7.2 \times 10^{-12} \exp(-3\ 250/R_gT)$
(4) $H + H + M \rightleftharpoons H_2 + M$	$1 \times 10^{-29}T^{-1}$
(5) $H + OH + M = H_2O + M$	$1 \times 10^{-28}T^{-1}$
(6) $OH + OH = H_2O + O$	$1 \times 10^{-11} \exp(-1\ 000/R_gT)$
(7) $OH + H_2 = H_2O + H$	$4 \times 10^{-11} \exp(-5\ 500/R_gT)$
(8) $CO + OH = CO_2 + H$	$5 \times 10^{-13} \exp(-600/R_gT)$
(9) $O + O + M = O_2 + M$	$1 \times 10^{-29}T^{-1}$
(10) $CO + O + M = CO_2 + M$	$2 \times 10^{-29}T^{-1} \exp(-4\ 000/R_gT)$
(11) $O + H_2 \rightleftharpoons OH + H$	$3 \times 10^{-11} \exp(-8\ 200/R_gT)$
(12) $H + O_2 = OH + O$	$3 \times 10^{-10} \exp(-16\ 500/R_gT)$
(13) $O + H + M = OH + M$	$1 \times 10^{-29}T^{-1}$
(14) $O + N_2 = NO + N$	$2.3 \times 10^{-10} \exp(-75\ 400/R_gT)$
(15) $N + O_2 = NO + O$	$1.1 \times 10^{-14}T \exp(-6\ 250/R_gT)$
(16) $NO + O + M = NO_2 + M$	$4.17 \times 10^{-33} \exp(+1\ 860/R_gT)$
(17) $NO + OH = NO_2 + H$	$2.8 \times 10^{-12} \exp(-30\ 000/R_gT)$
(18) $Cl + OH = HCl + O$	$3.0 \times 10^{-11} \exp(-9\ 900/R_gT)$
(19) $Cl + Cl + M = Cl_2 + M$	$1.6 \times 10^{-33} \exp(+1\ 600/R_gT)$
(20) Liquid water + $N_2 \rightarrow H_2O + N_2$	See text
(21) $N + N + M = N_2 + M$	$5.6\ E^{-30}T^{-1}$
(22) $H + CL_2 \rightleftharpoons HCl + Cl$	$2.0\ E^{-10}$

[a]Rate coefficient units are in terms of molecules, cm^3, sec. AlCl, $AlCl_2$, and Al_2O_3 are included in the plume as inert species. These rate coefficients are taken from reference 2.

TABLE IV.- SPACE SHUTTLE SOLID-ROCKET MOTOR EXIT

PLANE AVERAGE VALUES

[Space shuttle data obtained from Ben Shackleford, Marshall Space Flight Center, Mar. 1974]

Exit plane species	Mole fractions	Exit plane species	Mole fractions
AlCl	0.00003	H2	0.27812
$AlCl_2$	.00008	H_2O	.14068
$AlCl_3$	.00001	NO	.00001
AlOCl	.00002	N_2	.08401
Al_2O_3	.07975	O	.00001
CO	.23205	OH	.00046
CO_2	.02120	ClO	8.1×10^{-9}
Cl	.00225	Cl_2	6.9×10^{-7}
Fe	.00011	HO_2	1.2×10^{-10}
FeCl	.00001	NO_2	5.8×10^{-12}
$FeCl_2$	.00122	N_2O	8.6×10^{-11}
H	.00556	O_2	2.0×10^{-7}
HCl	.15442	N	0.0

Exit plane conditions based on an equilibrium model:

p_{exit}, atm	1.00
T_{exit}, K	2308
M_{exit}	2.779
r_{exit}, m	1.810
U_{exit}, m/sec	2433.8

TABLE V.- PLUME COMPOSITION AT 1 km DOWNSTREAM OF EXIT PLANE

$\left[k_f(T) = 10^{-16}\sqrt{T}\right]$

Entrained water flow/Original gas flow at exit planes	2.4	1.3	0.85	0.65
Species	Quantity of species, g/m			
HCl	23 146	22 206	21 831	21 405
H_2O	271 081	166 145	110 054	85 685
CO	360	97	76	69
CO_2	46 446	47 200	47 461	47 245
Al_2O_3	34 290	34 719	34 684	34 452
NO	20	628	1 207	1 805
Cl_2	977	1 990	2 457	2 689
Liquid water	63 162	15 100	5 072	4 218

TABLE VI.- PLUME COMPOSITION AT 1 km DOWNSTREAM OF EXIT PLANE

AS A FUNCTION OF REACTION RATE COEFFICIENT

FOR EXCESS WATER FLOW CASE

$\left[\text{Liquid water} + N_2 \rightarrow H_2O + N_2\right]$

$\frac{k_f(T)}{\sqrt{T}}$	10^{-20}	10^{-17}	10^{-16}	10^{-15}
Species	Quantity of species, g/m			
HCl	22 215	23 361	23 146	23 701
CO	157	303	360	2 307
CO_2	47 575	47 238	46 446	42 908
NO	171	16	20	3
Cl_2	2 144	1 014	977	3
Al_2O_3	34 778	34 826	34 290	33 936

TABLE VII.- FINAL PLUME COMPOSITION AS A FUNCTION OF TURBULENT MIXING

[$k_f(T) = 10^{-16\sqrt{T}}$; this table contains estimates of asymptotic values which will be slightly higher than the values of 1 km downstream]

α	1	5	10	20	100
Species	Quantity of species, g/m				
HCl	31 116	30 608	30 320	29 807	28 649
Cl_2	1 321	1 834	2 030	2 448	3 566
Cl	27	37	43	65	174
CO	487	547	554	615	974
CO_2	62 835	64 879	62 670	62 373	62 054
Al_2O_3	46 390	46 390	46 390	46 390	46 390
NO	27	18	17	16	15
H_2O	366 628	397 779	389 870	392 607	398 212
Liquid water	85 450	80 854	65 163	60 811	57 082

TABLE VIII.- QUANTITIES OF SPECIES FOR FREE FLIGHT CASE AND EXCESS WATER CASE WITH $\alpha = 5$ FOR SAME VELOCITY AND NOZZLE EXIT PLANE CONDITIONS

	Free flight	Combined effects
HCl, g/m	29 156	30 608
Cl_2, g/m	3 282	1 834
NO, g/m	2 029	18
CO, g/m	106	547

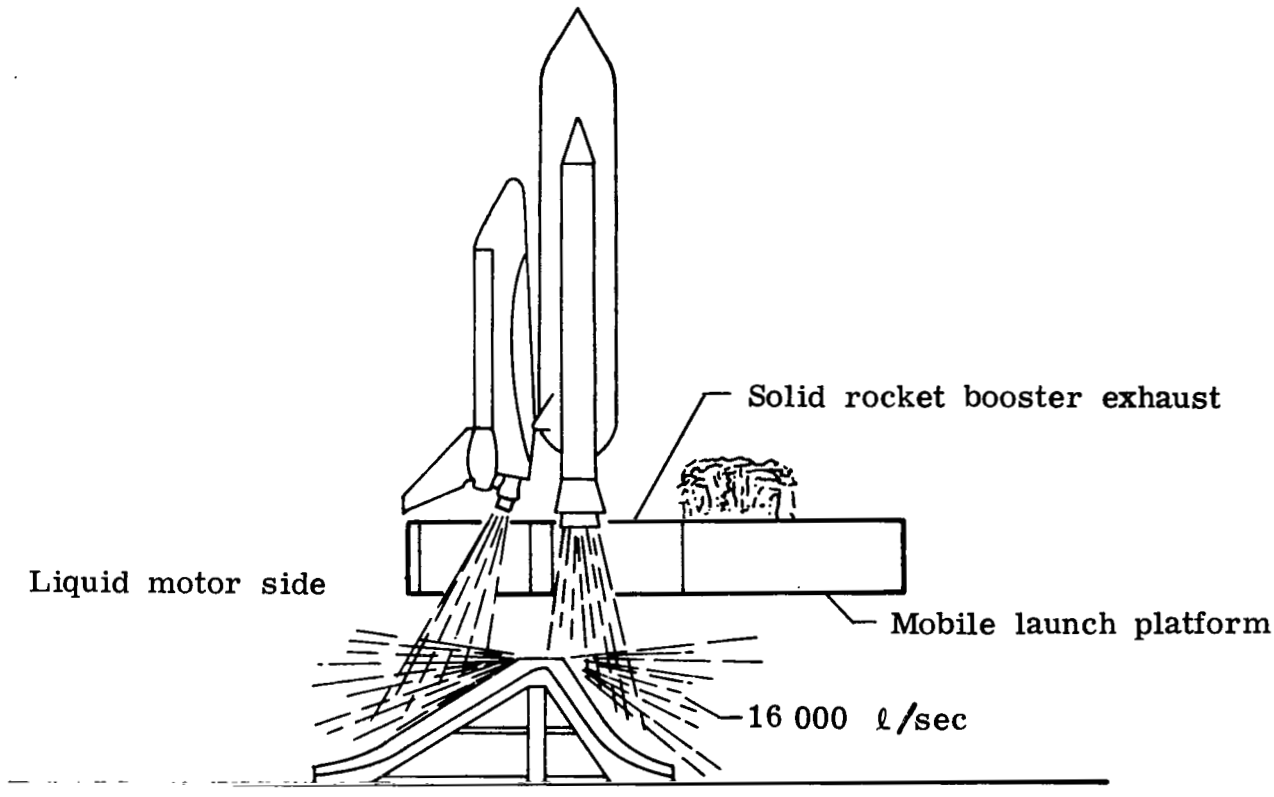

Figure 1.- Pad sound suppression scheme.

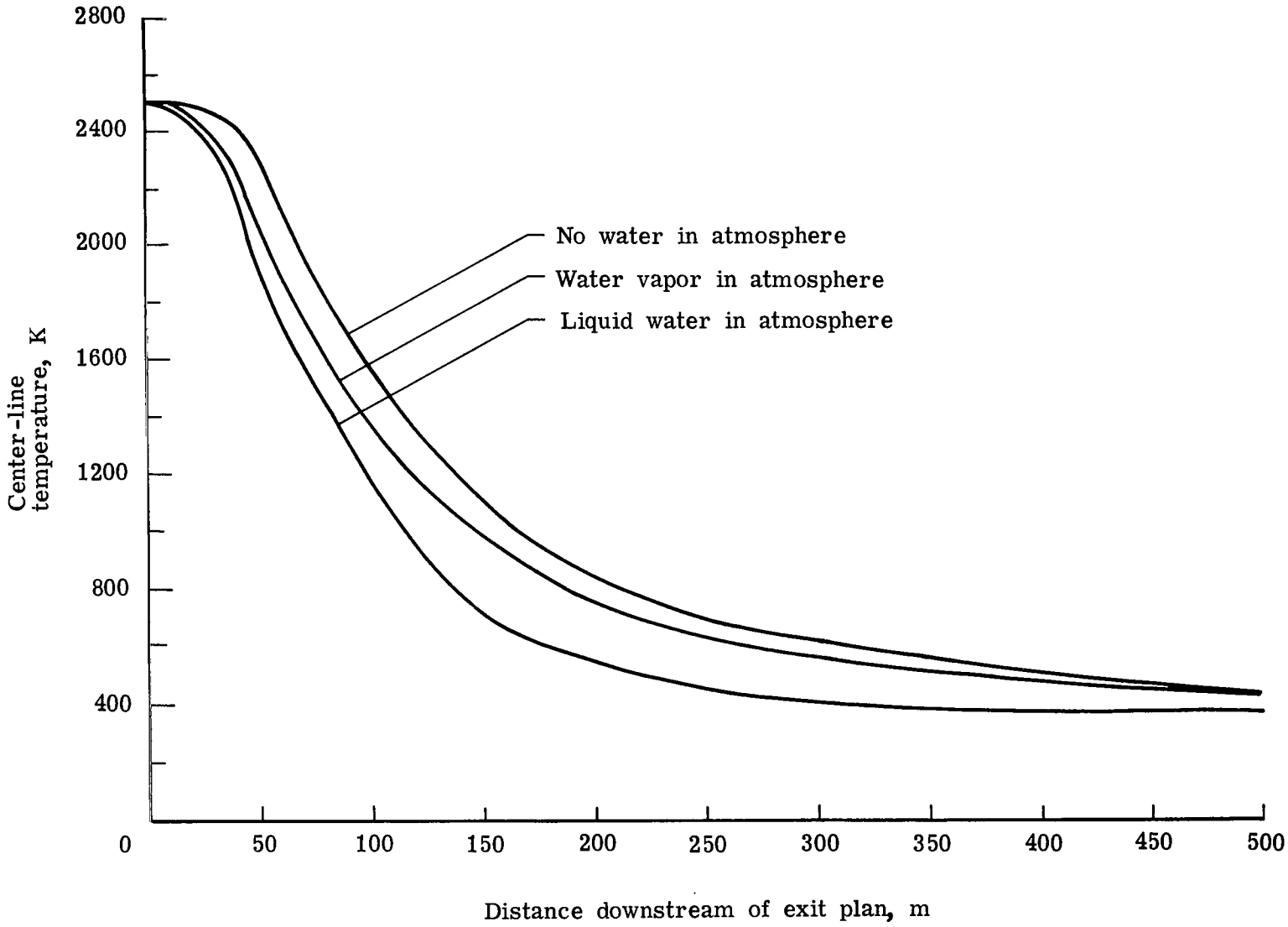

Figure 2.- Quenching effects of water on nonreacting shuttle-like plume. Amount of water used is very large and identical in both cases.

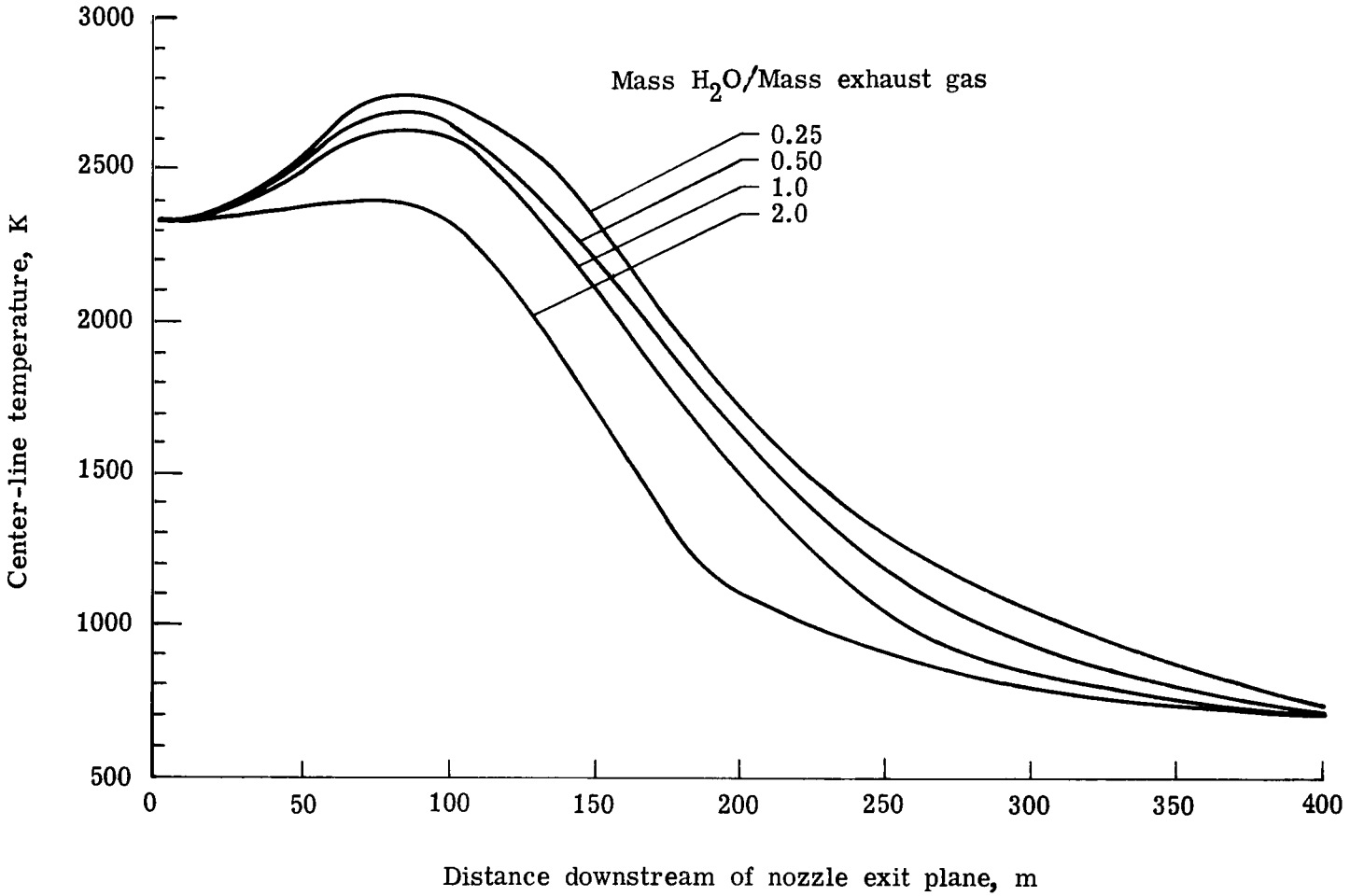

Figure 3.- Plume center-line temperature as a function of distance downstream of nozzle exit plane for various amounts of water entrained. Evaporation rate coefficient used is $10^{-16}\sqrt{T}$.

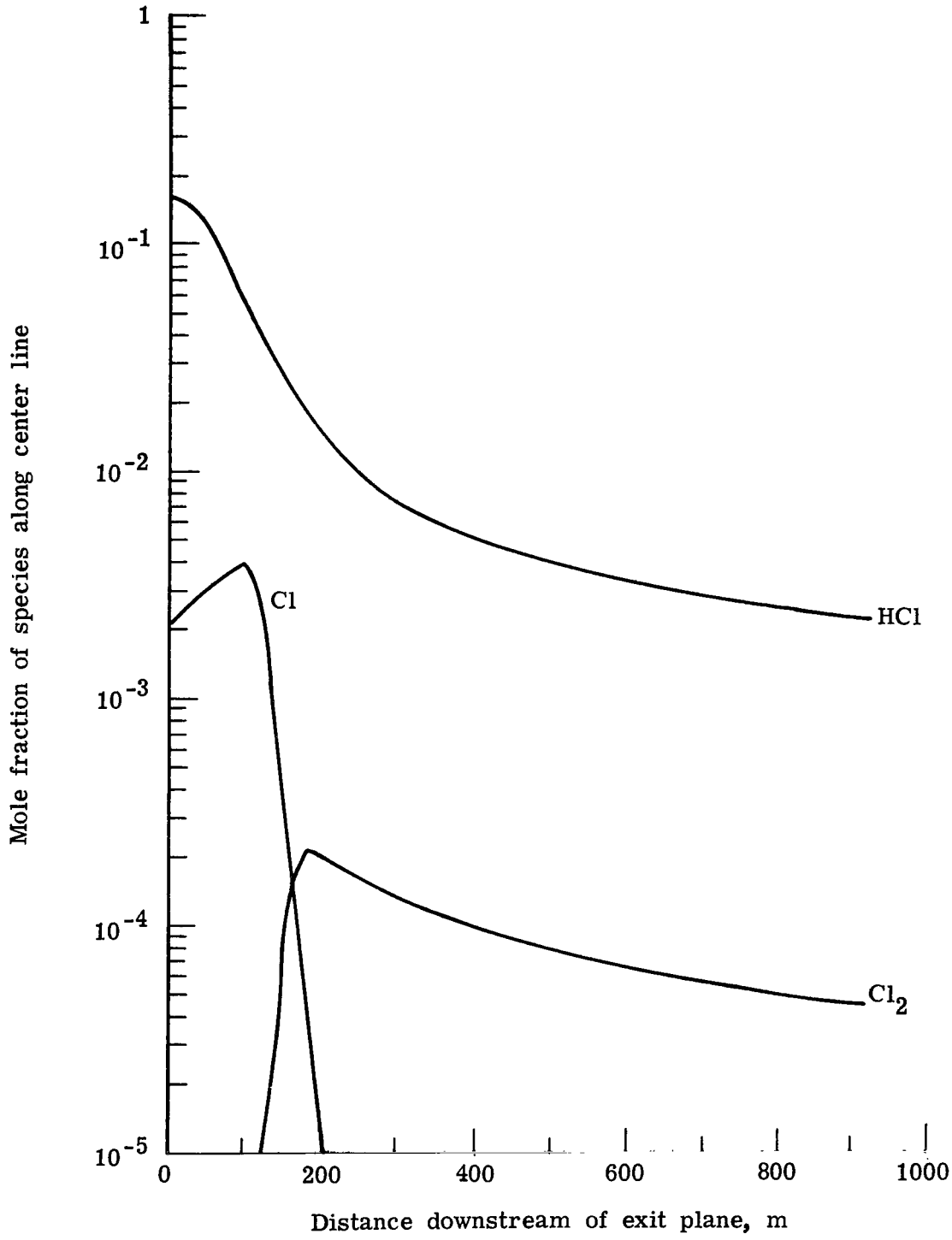

Figure 4.- Mole fractions of combustion products along plume center line as a function of distance downstream of nozzle exit plane. Rate coefficient used is $10^{-16}\sqrt{T}$. Excess flow case; Mass H_2O/Mass exhaust gas, 2.

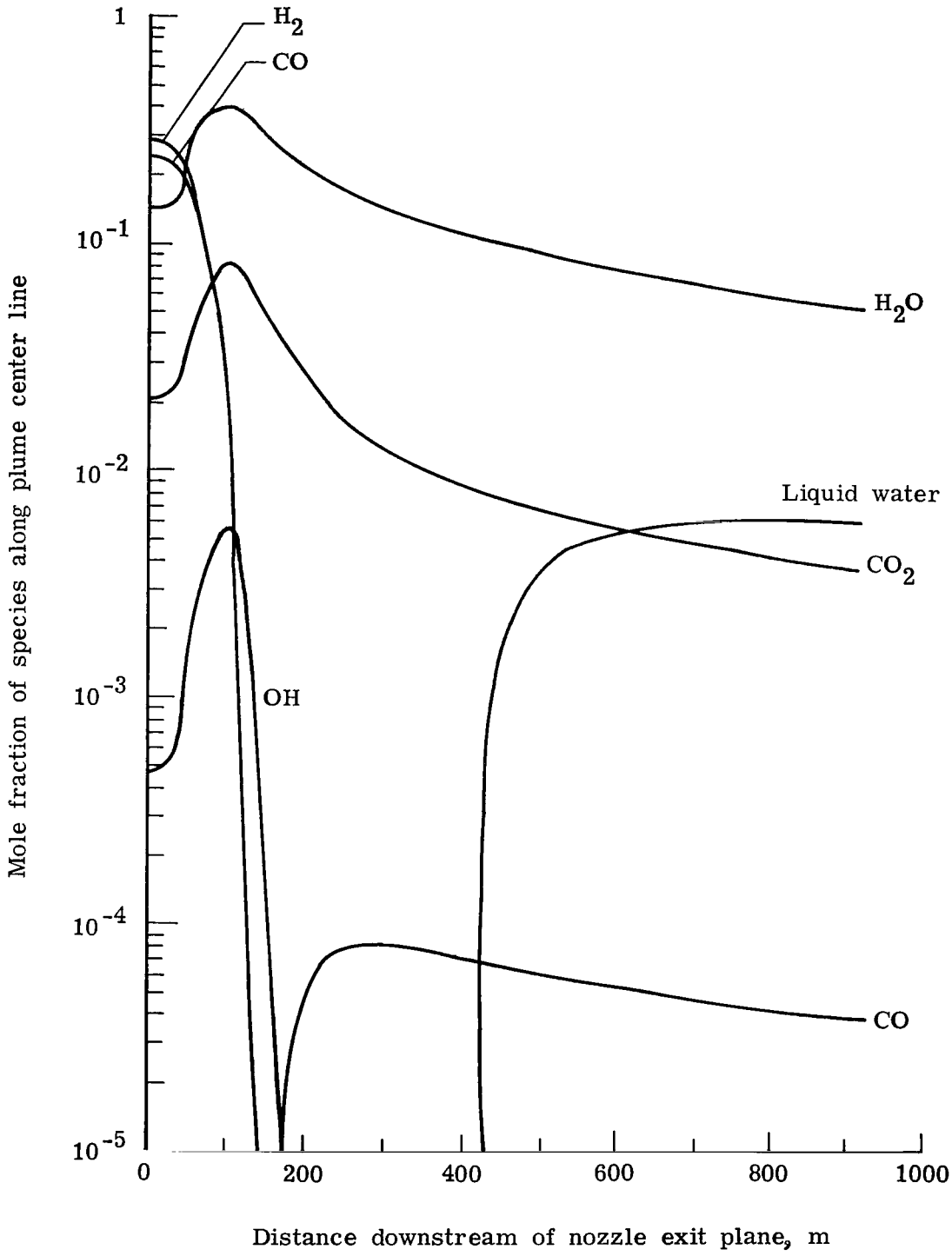

Figure 5.- Mole fractions of combustion products along plume center line as a function of distance downstream of nozzle exit plane. Rate coefficient used for water evaporation is $10^{-16}\sqrt{T}$. Mass H_2O/Mass exhaust gas, 2.

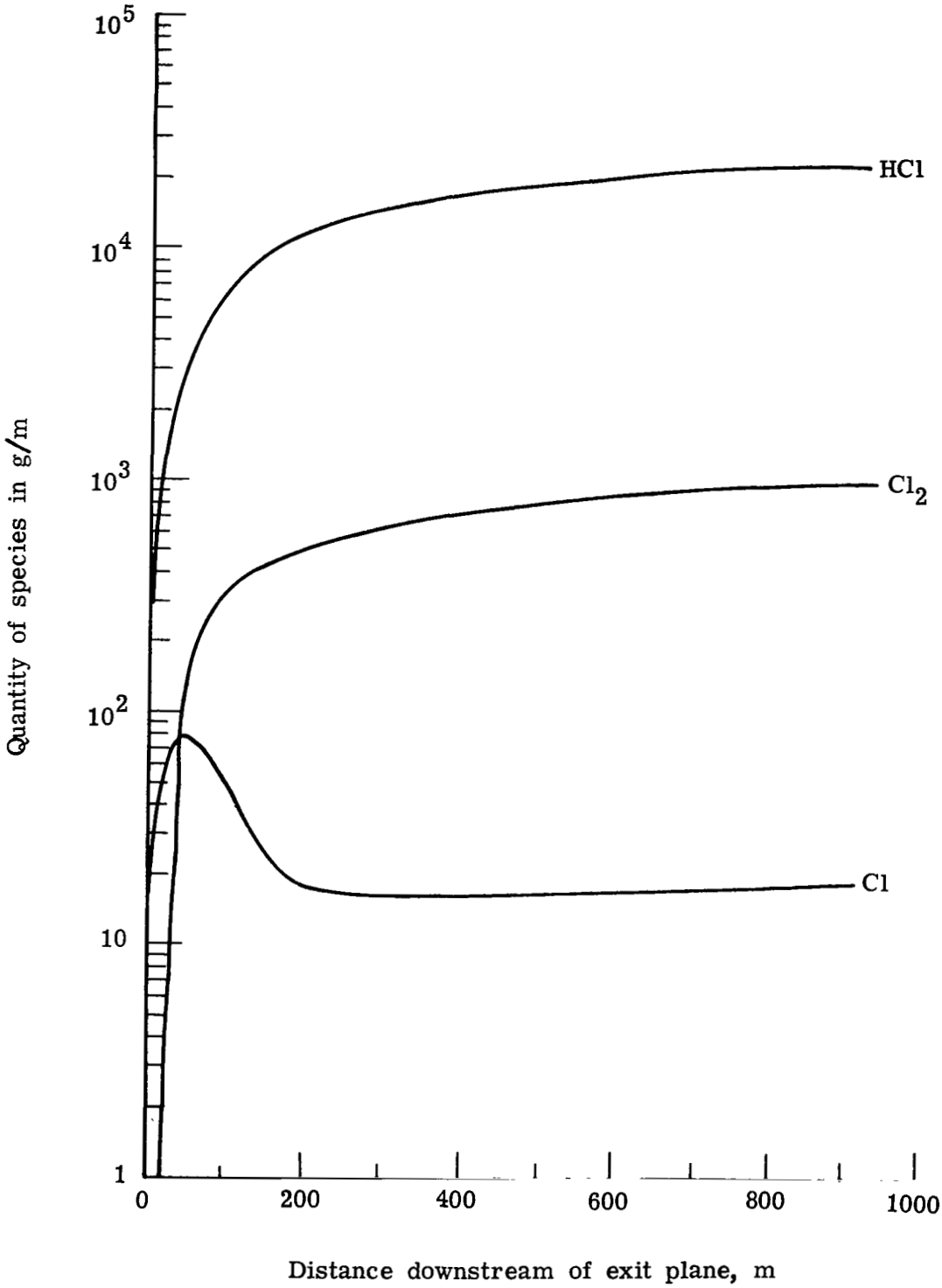

Figure 6.- Quantities of chlorine containing species (g/m) in plume as a function of distance downstream of nozzle exit plane. The evaporation rate coefficient used is $10^{-16}\sqrt{T}$. Mass H_2O/Mass exhaust products, 2.

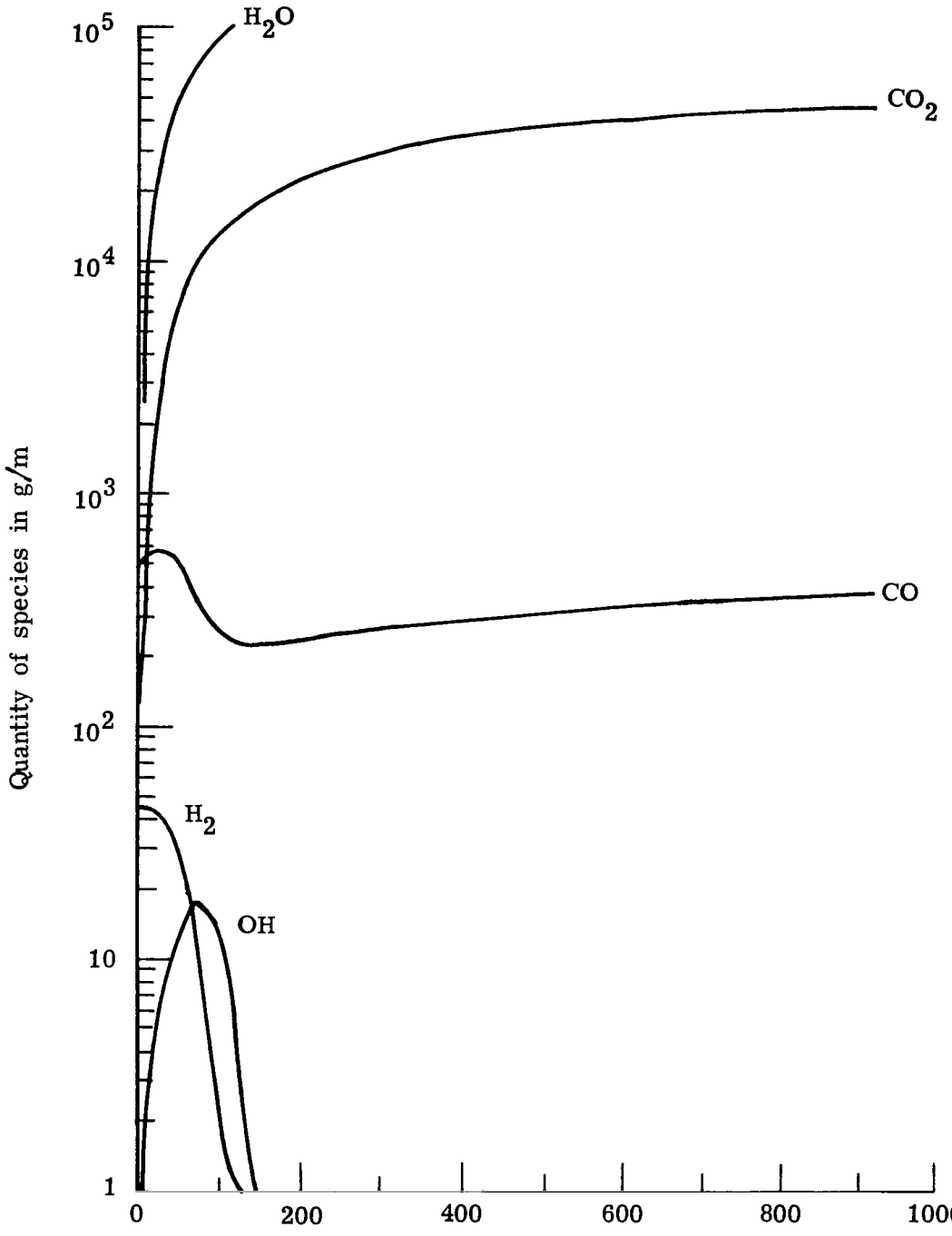

Figure 7.- Quantities of combustion products (g/m) in plume as a function of distance downstream of nozzle exit plane. Evaporation rate coefficient used is $10^{-16}\sqrt{T}$. Mass H_2O/Mass exhaust products, 2.

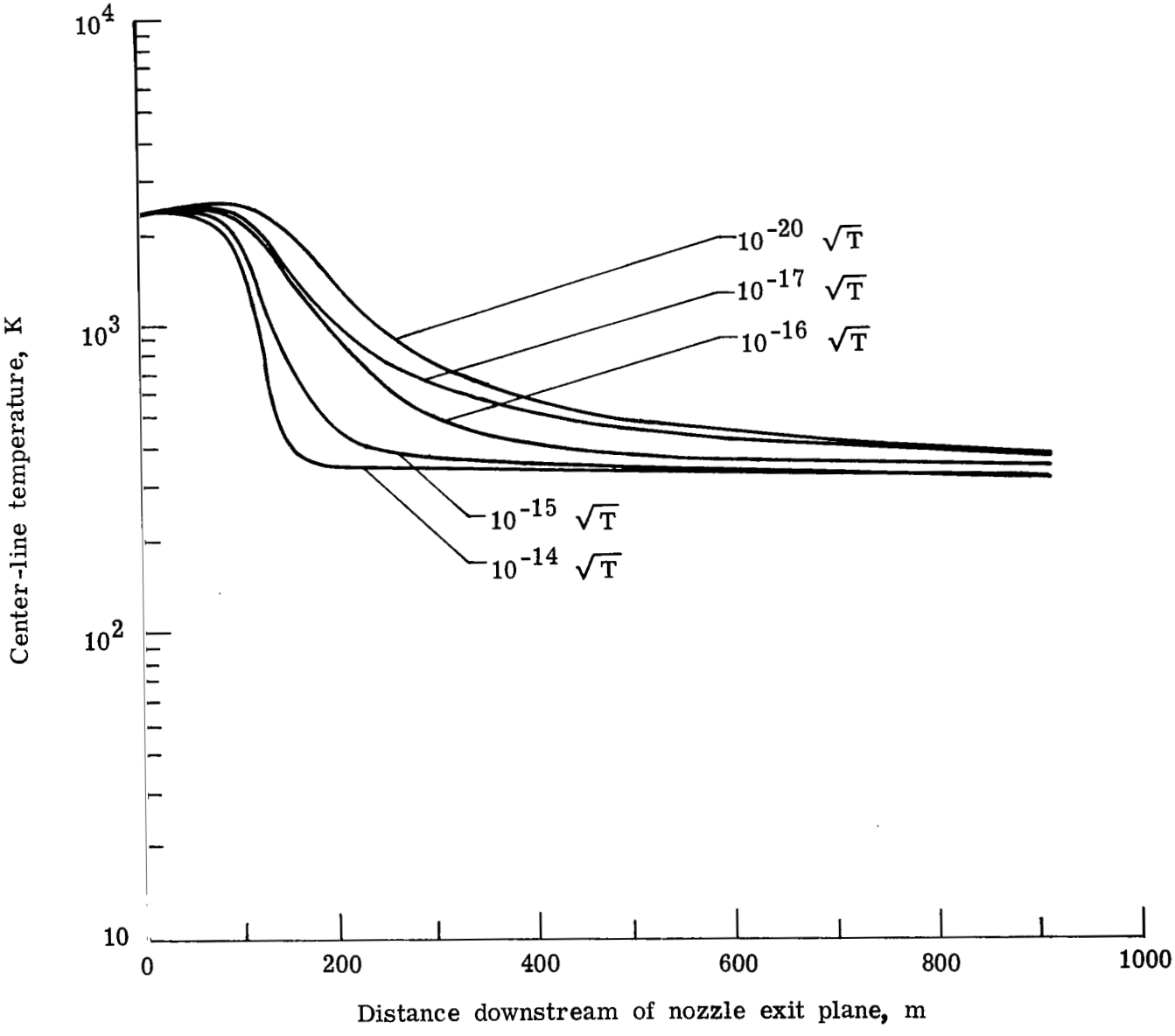

Figure 8.- Center-line temperature as a function of distance downstream of nozzle exit plane in excess water case for several evaporation rate coefficients. Mass H_2O/Mass exhaust gases, 2

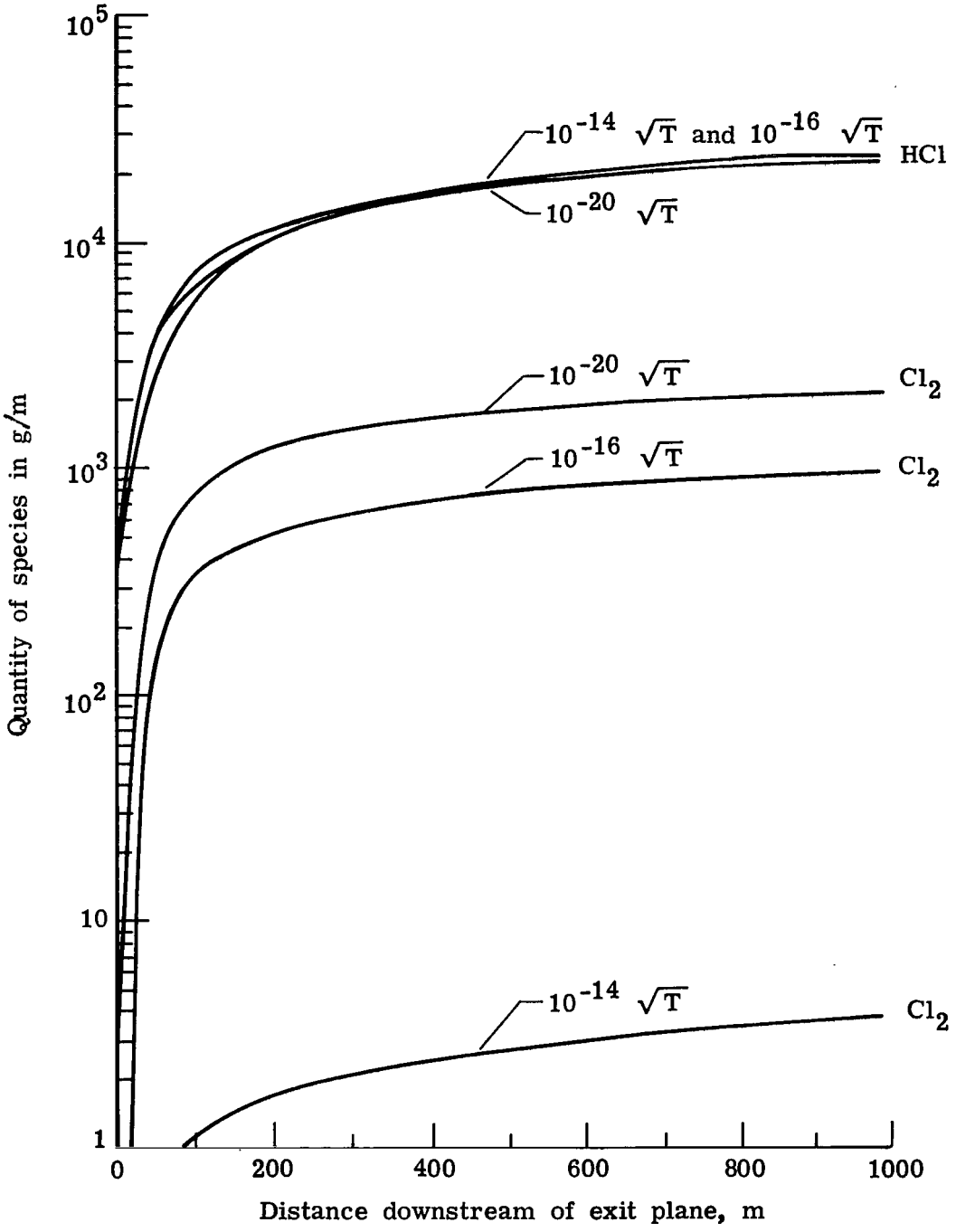

Figure 9.- Quantities of chlorine containing species in plume (g/m) as a function of distance. Downstream of nozzle exit plane for various evaporation rate coefficients. Excess water case (Mass H_2O/Mass exhaust = 2) is considered.

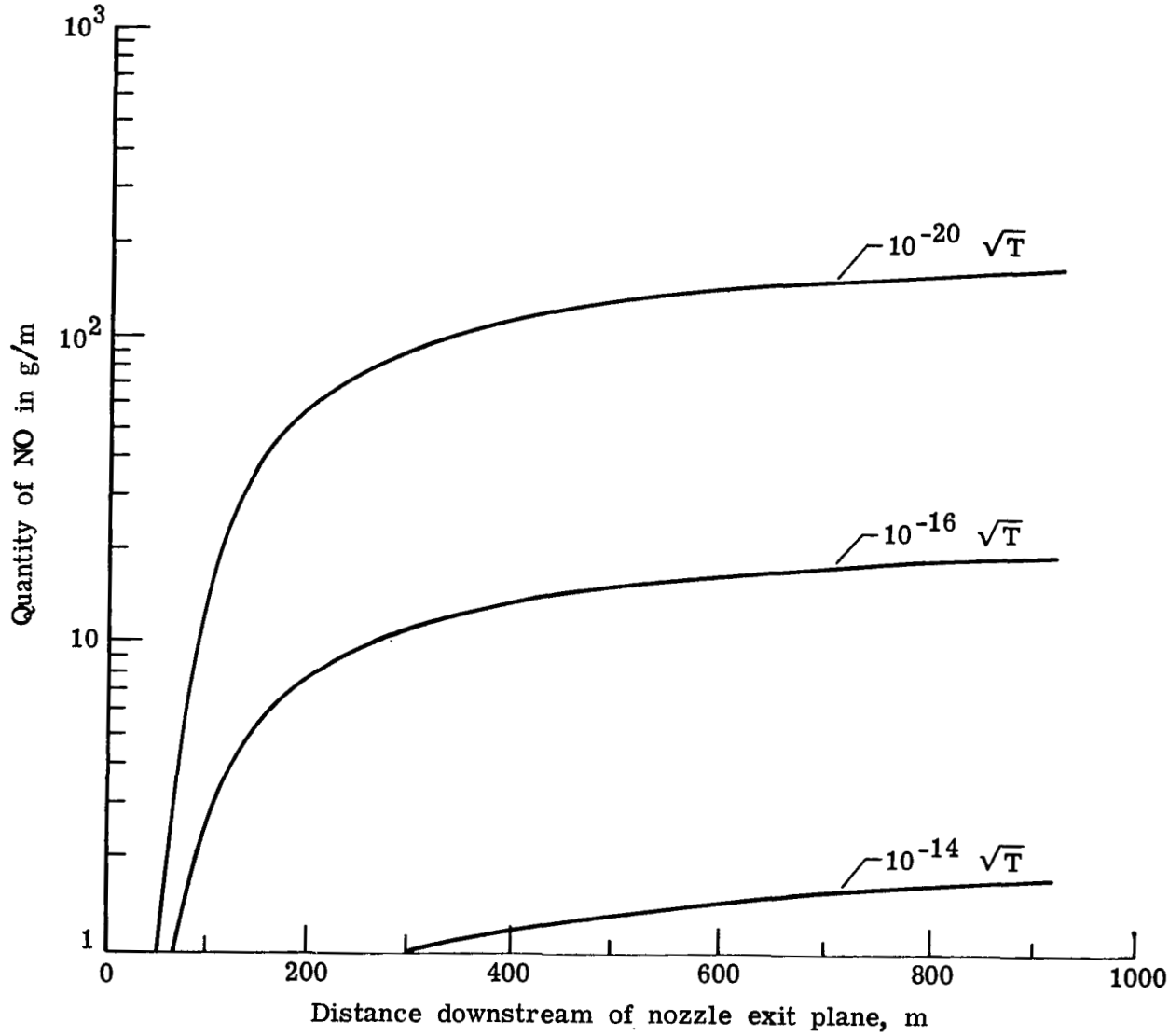

Figure 10.- Quantities of nitric oxide produced by using three alternate evaporation rate coefficients.

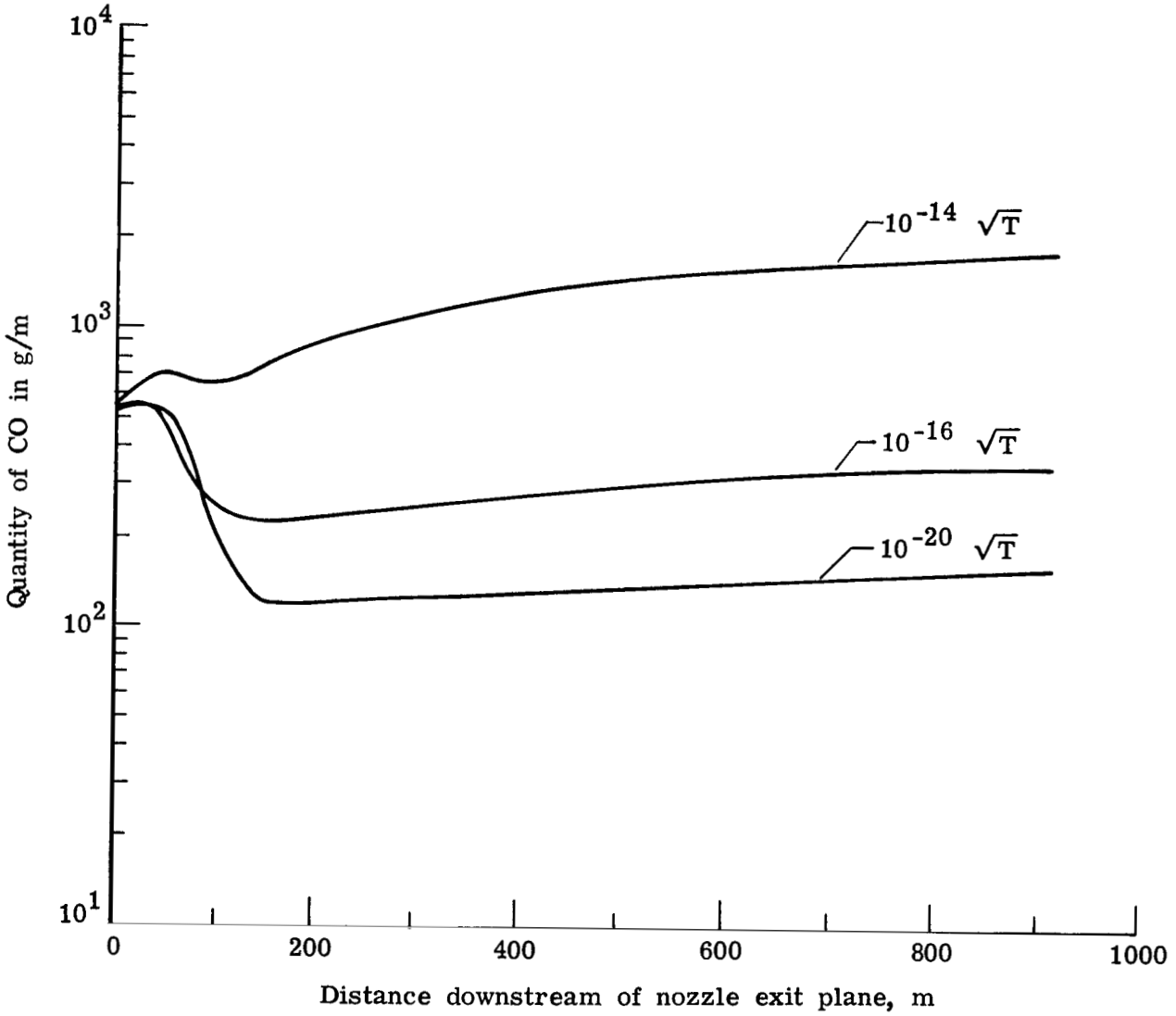

Figure 11.- Quantities of CO surviving after burning using three alternate evaporation rate coefficients.

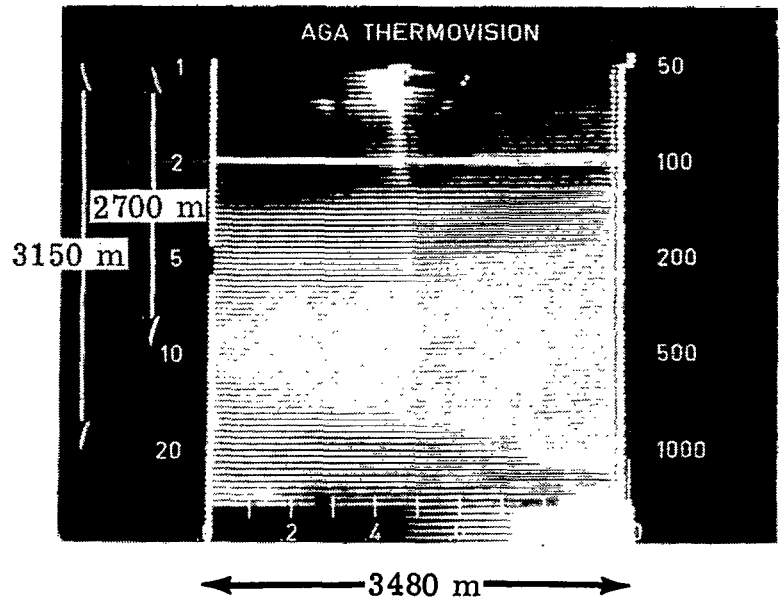

L-77-388

Figure 12.- Infrared scanner photograph of heat pattern from Titan III, March 14, 1976. Altitude approximately 3 km. Ambient clouds and ground form background intensities.

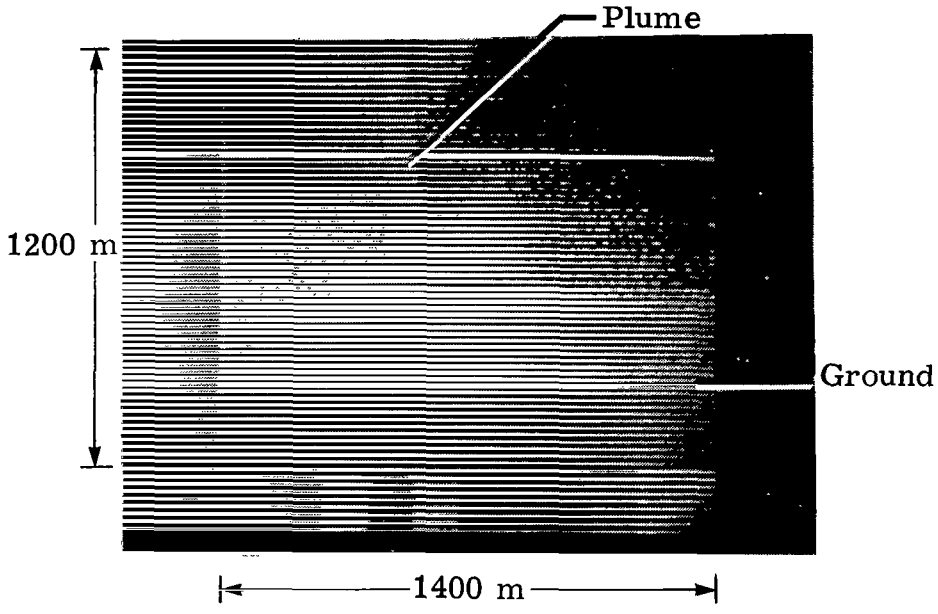

L-77-389

Figure 13.- Infrared scanner photograph of Titan III, May 20, 1975. Altitude approximately 1.1 km. 100 K above ambient (400 K) isotherm is shown for plume.

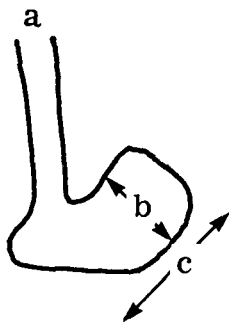

a = 80 m
b = 200 m
c = 280 m

(a) 400 K isotherm of plume in ordinary coordinates. $\epsilon = 0.5$.

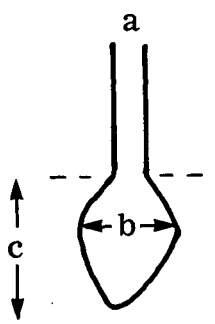

a = 80 m
b = 200 m
c = 280 m

(b) 400 K isotherm of same plume (idealized in downstream coordinate system).

Figure 14.- 400 K isotherms.

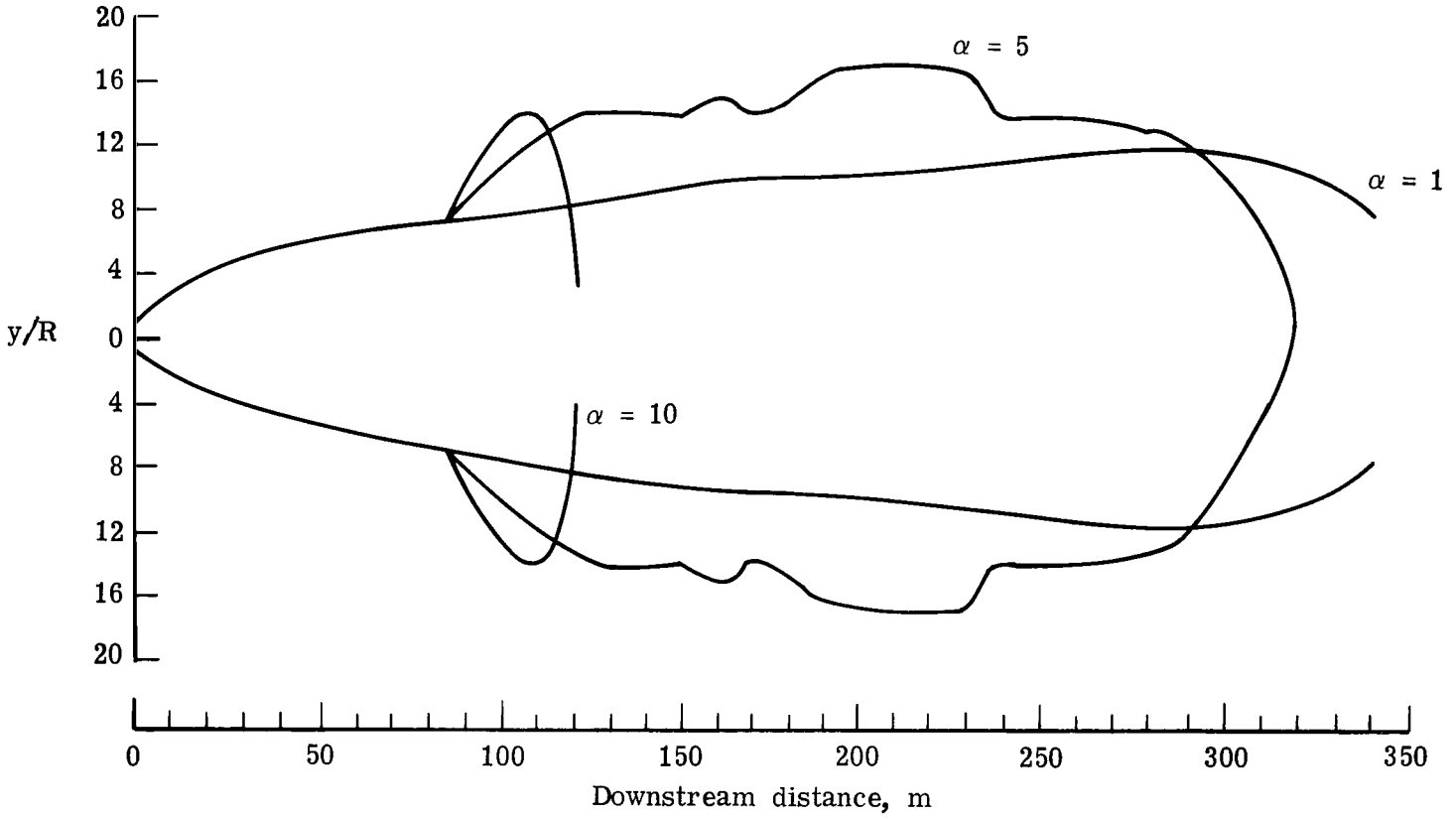

Figure 15.- 400 K isotherm for various turbulence parameters α. α = 1 in three cases until downstream distance reaches 80 m. R = 1.85 m; Mass of entrained H_2O/Mass exhaust, 0.25.

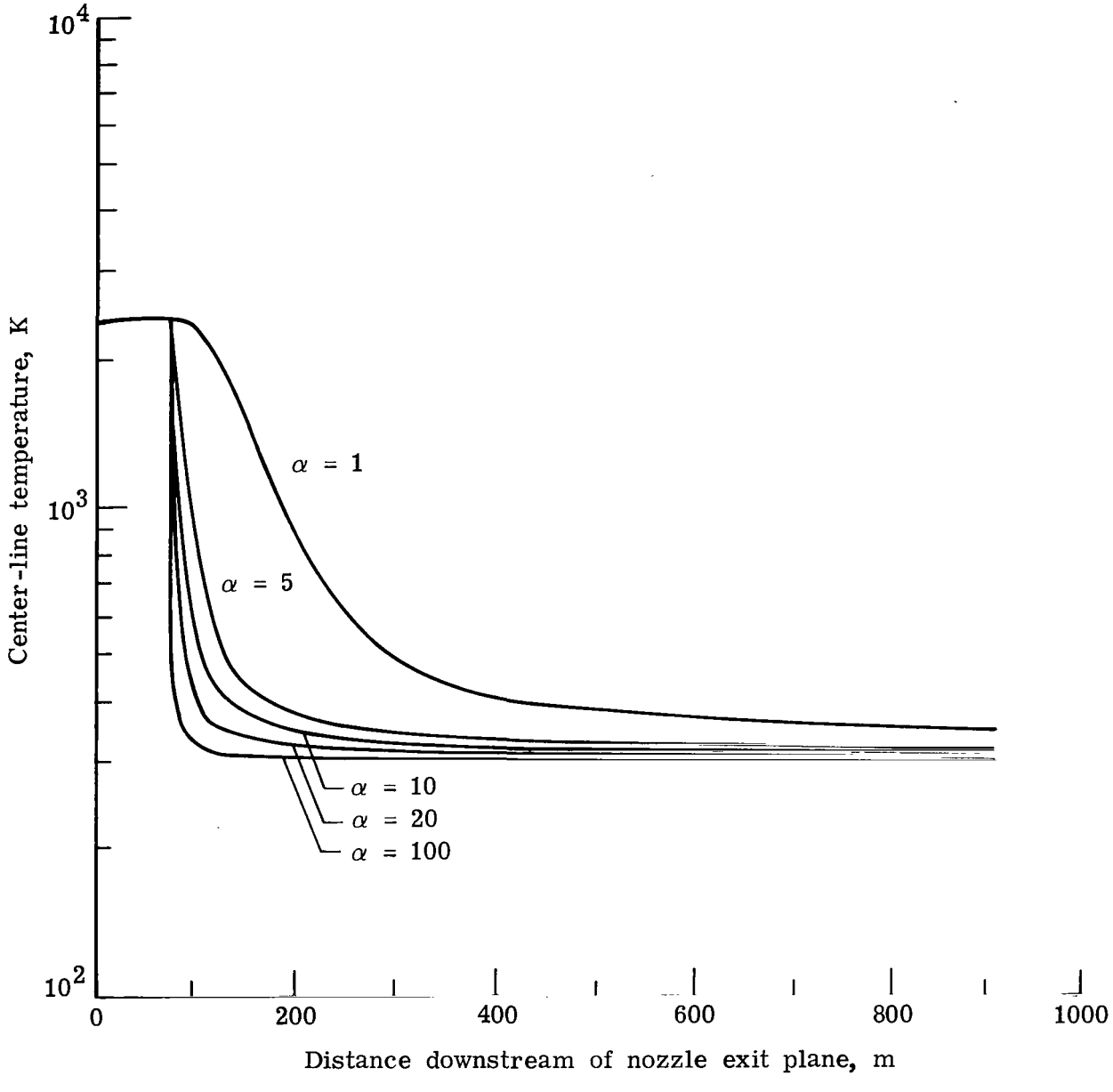

Figure 16.- Center-line temperature as a function of distance downstream of nozzle exit plane for several different turbulent mixing parameters.

1. Report No.	2. Government Accession No.	3. Recipient's Catalog No.
NASA TP-1111		

4. Title and Subtitle
EFFECTS OF ENTRAINED WATER AND STRONG TURBULENCE ON AFTERBURNING WITHIN SOLID ROCKET MOTOR PLUMES

5. Report Date
January 1978

6. Performing Organization Code

7. Author(s)
Richard I. Gomberg and Richard G. Wilmoth

8. Performing Organization Report No.
L-11875

9. Performing Organization Name and Address
NASA Langley Research Center
Hampton, VA 23665

10. Work Unit No.
506-21-30-01

11. Contract or Grant No.

12. Sponsoring Agency Name and Address
National Aeronautics and Space Administration
Washington, DC 20546

13. Type of Report and Period Covered
Technical Paper

14. Sponsoring Agency Code

15. Supplementary Notes

16. Abstract

During the first few seconds of the space shuttle trajectory, the solid rocket boosters will be in the proximity of the launch pad. Because of the launch pad structures and the surface of the Earth, the turbulent mixing experienced by the exhaust gases will be greatly increased over that for the free-flight situation. In addition, a system will be present, designed to protect the lifting vehicle from launch structure vibrations, which will inject large quantities of liquid water into the hot plume. This report studies the effects of these two phenomena on the temperatures, chemical composition, and flow field present in the afterburning solid rocket motor exhaust plumes of the space shuttle. The study includes results from both a computational model of the afterburning and supporting measurements from Titan III exhaust plumes taken at Kennedy Space Center with infrared scanning radiometers.

17. Key Words (Suggested by Author(s))
Afterburning
Space shuttle
Launch vehicle effluents

18. Distribution Statement
Unclassified - Unlimited

Subject Category 45

19. Security Classif. (of this report)	20. Security Classif. (of this page)	21. No. of Pages	22. Price*
Unclassified	Unclassified	36	$4.50

* For sale by the National Technical Information Service, Springfield, Virginia 22161

NASA-Langley, 1978

4 1 1U,A, 121277 S00903DS
DEPT OF THE AIR FORCE
AF WEAPONS LABORATORY
ATTN: TECHNICAL LIBRARY (SUL)
KIRTLAND AFB NM 87117